JOURNAL OF GEOPHYSICAL RESEARCH, VOL. 106, NO. D12, PAGES 12,489–12,497, JUNE 27, 2001

Estimating the cloudy-sky albedo of sea ice and snow from space

Jeffrey R. Key,[1] Xuanji Wang,[2] Julienne C. Stoeve,[3] and Charles Fowler[4]

Abstract. While satellites provide the means to monitor the temporal and spatial variability of surface albedo, their use has been limited to clear-sky areas because clouds obscure the surface at wavelengths in the solar spectrum. However, the effect of clouds on the surface albedo, especially that of snow and ice, is significant and should be considered in satellite retrievals. In this paper theoretical and observational evidence is given that shows the snow/ice albedo to be on the average 4-6% (absolute) higher under cloud cover than for clear skies, with a range of slightly less than 0 to approximately 15%. A method for retrieving the clear-sky broadband albedo of snow/ice from the advanced very high resolution radiometer is presented, and an adjustment for cloud optical depth is proposed. The cloudy-sky adjustment is independent of sensor type and could also be used with nonsatellite data sets. An application of the algorithm to data from the Surface Heat Budget of the Arctic Ocean experiment demonstrates that clear- and cloudy-sky snow surface albedo can be obtained from space with an uncertainty of approximately 7% absolute. While it may be sufficient to adjust a monthly clear-sky surface albedo climatology for clouds by incorporating the mean cloud effect of approximately 5%, adjustments for cloud optical depth should be performed with instantaneous retrievals.

1. Introduction

The extent to which the surface reflects incoming solar radiation is a critical factor in the surface radiation balance and the surface energy balance overall. The degree of reflection is commonly expressed as the ratio of upwelling to downwelling shortwave fluxes and is termed the "albedo." Surface albedo varies by surface type, surface conditions, solar zenith angle, and atmospheric composition. The broadband (solar spectrum) albedo of unfrozen ocean is between 0.05 and 0.2 (5-20%), depending on the solar zenith angle. Vegetation albedo is of the order of 0.1, depending on the vegetation state, soil type, and soil moisture content. Snow albedo varies from 0.5 to 0.9 and is strongly affected by the illumination angle, grain size, and soot content, which are largely a function of age. In the Arctic the albedo of the sea ice pack can vary from 0.1 for open water portions, to 0.2-0.3 for melt ponds on the ice, to 0.9 for fresh snow cover.

Satellites provide the ability to measure the spatial variability of surface albedo with reasonable time resolution. However, because the estimates are made using bands in the solar portion of the spectrum, retrievals are limited to clear-sky conditions. A number of procedures for the retrieval of clear-sky surface albedo from satellite data have been developed. *DeAbreu et al.* [1994] presented and applied an algorithm for the retrieval of clear-sky sea ice albedo, as did *Lindsay and Rothrock* [1994]. *Stroeve et al.* [1997] developed a method for the retrieval of snow albedo over the Greenland ice sheet. *Csiszar and Gutman* [1999] describe two algorithms for estimating snow-free land surface albedo. These four methods utilized data from the advanced very high resolution radiometer (AVHRR) on board NOAA polar orbiting satellites. Other sensors have also been used. For example, *Hall et al.* [1990] estimated snow reflectance in a narrow band using the Landsat Thematic Mapper, while *Li and Garand* [1994] estimated the surface broadband albedo for areas outside of the polar regions from Earth Radiation Budget Experiment (ERBE) top-of-atmosphere albedo. Land surface albedo is also being retrieved from the recently launched Moderate-Resolution Imaging Spectroradiometer [*Wanner et al.*, 1997].

Clouds influence the broadband surface albedo as a result of relative differences in absorption by snow, vegetation, and cloud liquid droplets or ice crystals at visible and near-infrared wavelengths. As will be shown later, the effect is significant and of opposite sign for different surfaces. Clouds increase the broadband albedo of snow, but they tend to decrease that of vegetation. In areas of persistent cloudiness such as the Arctic, where cloud cover is typically 60-90%, relatively poor spatial coverage is obtained from clear-sky retrievals alone. Given that the effect of clouds on the surface albedo is significant and that cloud cover obscures a large portion of the surface in many regions, a method of estimating the cloudy-sky surface albedo is needed.

The purpose of this paper is to demonstrate the effect of clouds on the broadband albedo of sea ice and snow-covered surfaces and to present and apply a method for estimating the cloudy-sky albedo with the AVHRR. The procedure interpolates clear-sky albedo retrievals to cloudy areas, then adjusts

[1]Office of Research and Applications, National Environmental Satellite, Data, and Information Service, NOAA, Madison, Wisconsin.
[2]Cooperative Institute for Meteorological Satellite Studies, University of Wisconsin, Madison, Wisconsin.
[3]Cooperative Institute for Research in Environmental Sciences, University of Colorado, Boulder, Colorado.
[4]Colorado Center for Astrodynamics Research, University of Colorado, Boulder, Colorado.

Paper number 2001JD900069.
0148-0227/01/2001/JD900069$09.00

them for cloud cover using satellite estimates of cloud optical depth. For completeness a clear-sky retrieval procedure is presented that is similar to that developed for land surfaces by *Csiszar and Gutman* [1999] and a potential improvement over the methods described by *DeAbreu et al.* [1994] and *Lindsay and Rothrock* [1994]. It will be shown that the effect of clouds is to increase the broadband albedo of snow and ice and that the magnitude of the change can be estimated as a function of the clear-sky albedo, cloud optical depth, and the solar zenith angle. While the effect of clouds on the surface albedo of snow has been observed by others [cf. *Grenfell and Perovich,* 1984], here we examine it in detail both theoretically and empirically. The geographic focus is on the polar regions, though the problem applies to snow and ice surfaces at any latitude.

2. Effect of Clouds on Surface Albedo

2.1. Theoretical Effects

Clouds affect the broadband surface albedo primarily because their absorptivity varies as a function of wavelength in a manner different from that of the surface. Clouds absorb little in the visible portion of the electromagnetic spectrum (around 0.6 μm) but absorb a significant proportion of near-infrared and solar-infrared radiation (2-4 μm). This is illustrated in Figure 1, which shows the imaginary index of refraction for water and ice and the single-scattering albedo of liquid (hereinafter "water") cloud for two different effective radii. The imaginary part of the index of refraction is a measure of absorptivity; as the index value increases so does the degree of absorption. The single-scattering albedo is the ratio of the scattering and extinction coefficients and is therefore an indication of how effectively a volume of particles scatter. It decreases as scattering decreases and as absorption increases.

Figure 2 gives the spectral albedo of old snow, fresh snow, bare sea ice, and vegetation. As *Li and Garand* [1994] illustrate, vegetation albedo is only weakly dependent upon solar

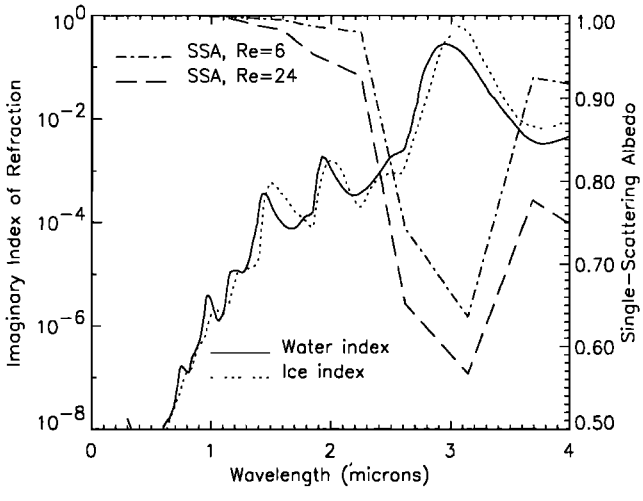

Figure 1. The imaginary index of refraction for water and ice (left axis) and the single-scattering albedo (SSA) of water cloud (right axis) as a function of wavelength over the solar portion of the spectrum. The single-scattering albedo is shown for two different effective radii (Re, microns). The liquid water content of the cloud is 0.4 g m^{-3}.

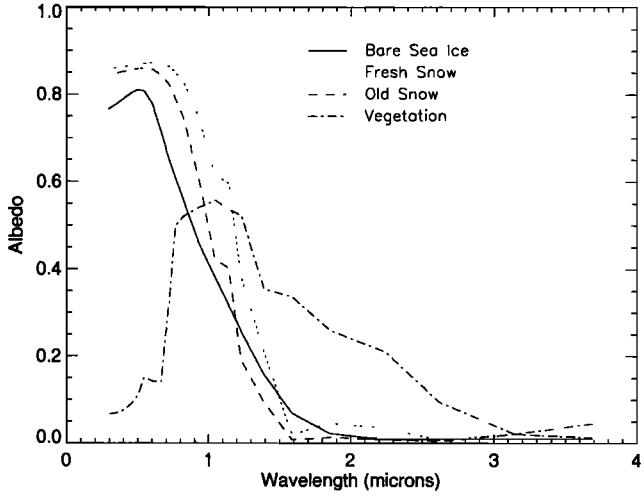

Figure 2. Spectral albedo of various surface types. Snow and sea ice albedos are based on a solar zenith angle of 60°.

zenith angle while snow albedo shows a strong dependence. The snow albedo data given in Figure 2 and used in radiative transfer calculations in this study is a function of solar zenith angle but vegetation albedo is not. Vegetation albedo is the mean of the albedos of grass, dry grass, deciduous forest, and coniferous forest [*Key and Schweiger,* 1998, and references therein]. Vegetation reflects little at visible wavelengths compared to snow but reflects a relatively large proportion of near-infrared radiation. Figure 1 implies that clouds will increase the proportion of visible to total radiation that reaches the surface, the net effect of which is to increase the proportion of total radiation reflected by snow because snow reflects strongly at visible wavelengths. For vegetation the effect is opposite, where the proportion of total radiation reflected decreases under clouds because vegetation absorbs more in the visible portion relative to the near infrared.

These effects are shown theoretically in Figure 3. The radiative transfer model Streamer [*Key and Schweiger,* 1998] was used for the calculations. Downwelling and upwelling radiative fluxes in the range of 0.28 - 4.0 μm were computed using a two-stream solver for two solar zenith angles, two albedos each for snow and vegetation, and a range of visible cloud optical depths, zero being clear. In the cloudy cases a water cloud was used with its top at the 500 hPa level, a water content of 0.2 g m^{-3}, and an effective droplet radius of 10 μm. Temperature and humidity profiles were based on a mean Arctic summer atmosphere with 25 layers. Total column aerosol visible (0.6 μm) optical depth was 0.1 with the Arctic haze optical model of *Blanchet and List* [1983].

The figure shows the ratio of cloudy to clear albedos so that a ratio greater than 1 indicates that the cloudy-sky albedo exceeds the clear-sky albedo. As stated above, the vegetation albedo model does not vary with solar zenith angle, so the zenith angle dependence of vegetation albedo in the figure occurs because of scattering effects in the atmosphere. As expected, snow albedo increases as cloud optical thickness increases. Vegetation albedo increases initially then decreases with increasing cloud thickness, particularly for the lower albedo case. For snow the ratio translates into absolute albedo differences in the range of 0.03 to 0.05 for cloud optical depths

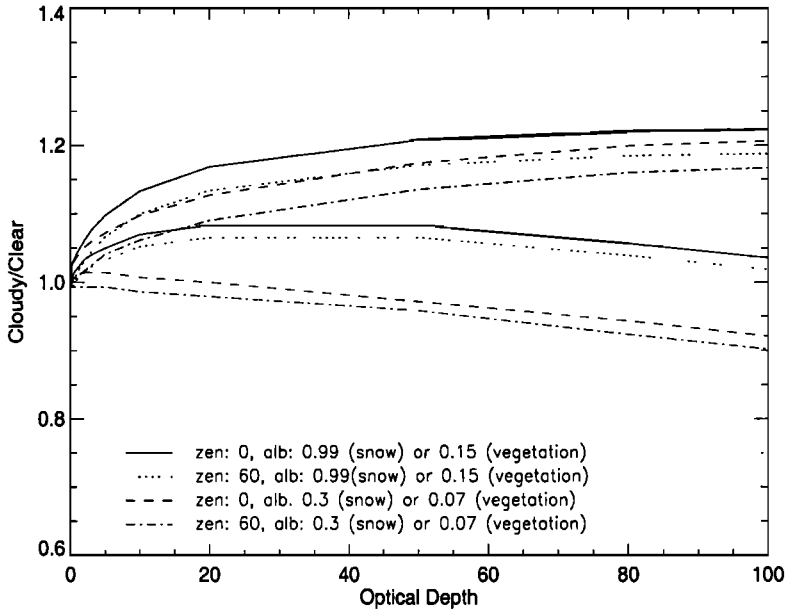

Figure 3. Differences between clear and cloudy surface albedos expressed as a fraction (cloudy divided by clear; 1 means no difference) for snow (top set of lines) and generic vegetation (bottom set), given as a function of cloud optical depth. Results were generated with a radiative transfer model for water and ice cloud under varying atmospheric conditions. The lines are for different solar zenith angles (0° and 60°) and visible surface albedos (0.3 and 0.99 for snow; 0.07 and 0.15 for vegetation).

less than 50 and 0.04 to 0.08 for optical depths between 50 and 100. The figure illustrates that the sensitivity of surface albedo to changes in cloud thickness is greatest for thin clouds.

2.2. Observed Effects

The effect of clouds on snow albedo has also been observed in the field. *Grenfell and Perovich* [1984] observed that for relatively thin Arctic clouds the albedo is about 0.05 higher than the clear-sky albedo. Surface measurements collected during the year-long Surface Heat Budget of the Arctic Ocean (SHEBA) project [*Moritz et al.*, 1993] produce similar results. During SHEBA, a Canadian icebreaker was frozen into the sea ice north of Alaska in October 1997 and drifted with the ice for 1 year. The ship's starting location was 75°N latitude and 143°W longitude, about 300 miles north of Deadhorse, Alaska. At the end of the experiment the ship station was at 80°N and 166°W, about 400 miles northwest of starting point. Meteorological observations were made continuously by a variety of instruments. Upwelling and downwelling shortwave radiation were measured with Eppley Precision Spectral Pyranometer (PSP) radiometers (0.285 to 2.8 μm) operated by scientists from the National Oceanic and Atmospheric Administration's (NOAA) Environmental Technology Laboratory. Surface observers reported cloud amount every 6 hours. Here we use hourly average surface radiative fluxes and cloud amounts linearly interpolated to hourly increments.

While the clear and cloudy albedos shown in Figure 3 were calculated for exactly the same illumination, surface, and atmospheric conditions, this is not possible with surface measurements so isolating the effects of clouds is more difficult. For example, while it is possible to find clear and cloudy cases with the same solar zenith angle in different months, it is not likely that the surface conditions would be the same. Therefore the differences between adjacent runs of clear and cloudy cases in the time series were compared, where a run is a sequence of clear hourly observations followed by a run of cloudy observations. Because of persistent cloudiness in the Arctic less than 40 clear-cloudy runs were found during the March - October period.

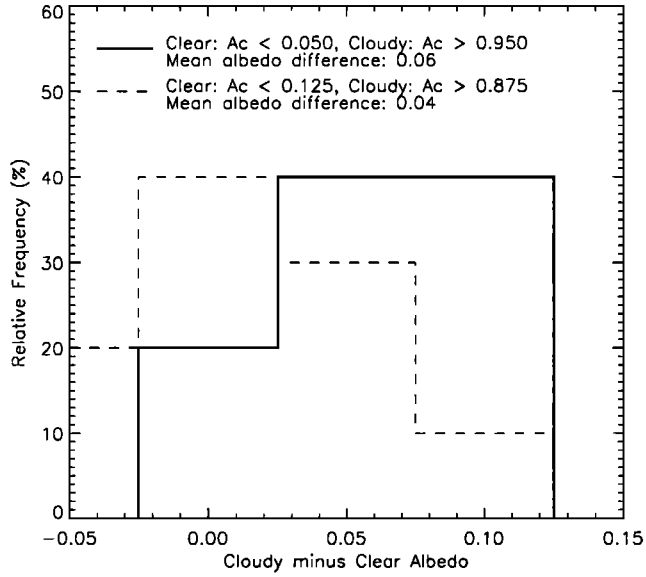

Figure 4. Relative frequency of differences between the broadband surface albedo for clear and cloudy adjacent runs of hourly observations made during SHEBA. Results are shown for two different cloud amounts (Ac) used to define "clear" and "cloudy" conditions. The resulting mean difference is given for each case.

Results are shown in Figure 4 for two different combinations of thresholds that define "clear" (less than 12.5% and 5% cloud cover) and "cloudy" (greater than 87.5% and 95%) observations. The histogram shows the relative frequency of differences between the means of the clear and cloudy albedos in each clear-cloudy sequence found in the surface observations. The cloudy-sky albedo exceeds the clear-sky value on average by 0.04 to 0.06 (4-6% absolute), though differences may exceed 0.1. The differences are largest for thicker cloud and clearer (lower cloud amount threshold) cases. Some negative differences do occur. An examination of those cases showed them to be the result of measurement error at very large solar zenith angles and instances where the snow characteristics changed in response to rapid warming or cooling events. The results shown in Figure 4 agree qualitatively and quantitatively with the model calculations of Figure 3.

3. Satellite Retrieval Methodology

The AVHRR has five channels centered at approximately 0.6, 0.9, 3.7, 11, and 12 μm (channels 1 through 5, respectively). Channels 1 and 2 are used to retrieve the clear-sky albedo, and channels 3, 4, and 5 are used indirectly in the cloudy-sky adjustment. The retrieval of the surface albedo with this instrument involves four steps: (1) convert channels 1 and 2 narrowband reflectances to a broadband reflectance, (2) correct the top-of-atmosphere (TOA) broadband reflectance for anisotropy, (3) convert the TOA broadband albedo to a surface broadband albedo, and (4) adjust the surface clear-sky broadband albedo for the effects of cloud cover in cloudy pixels.

The focus of this paper is on the last step, the estimation of the cloudy-sky albedo. Because this requires the use of a clear-sky albedo estimate, for completeness we provide one potential method of retrieving the clear-sky albedo. Alternative methods for each of steps 1-3 may be used, and some are noted in the discussions that follow.

The general methodology described by steps 1-3 was used by *Csiszar and Gutman* [1999] for global land studies. DeAbreu et al. [1994] and *Lindsay and Rothrock* [1994] used a procedure for snow/ice where the anisotropic reflectance correction was applied to channels 1 and 2, an atmospheric correction was done on those channels, then narrowband albedos were converted to broadband. We found that such a procedure tends to overestimate the albedo of snow/ice.

At this point a distinction should be made between "inherent" and "apparent" surface broadband albedos. The inherent albedo is the true, no-atmosphere, or "black-sky" albedo of the surface and is independent of changes in atmospheric conditions [cf. *Wanner et al.*, 1997]. However, Rayleigh scattering, gaseous absorption, and scattering and absorption by aerosols change the spectral distribution of radiation that reaches the surface, so that even in cloud-free conditions the amount of solar radiation reflected by the surface will depend on the atmospheric conditions and the spectral albedo signature of the surface. This effect is analogous to that of clouds illustrated in Figures 1-3. Because the atmosphere is ubiquitous, the apparent albedo is what we measure by up- and down-looking radiometers in the field.

Both the apparent and inherent albedos are functions of the solar zenith angle and are directional in that regard. The difference between them is very small for the ocean but can be relatively large for vegetation and snow. Figure 5 gives an example of the difference between the two albedo types for unfrozen ocean, vegetation, and snow, showing a range of modeled albedos at two solar zenith angles. As the figure illustrates, differences can be up to 10%, the greatest differences occurring with a low Sun angle over a bright surface. The effect of gases, primarily water vapor, is to increase the difference between the apparent and inherent albedos of snow (apparent greater than inherent), but to slightly decrease the difference for vegetation. Aerosols and Rayleigh scattering tend to decrease the apparent albedo of snow at larger zenith angles but increase the apparent albedo of vegetation. In both cases the apparent albedo exceeds the inherent albedo, but the difference between them decreases over snow and increases over vegetation as the solar zenith angle increases. As with clouds, the effects are the result of differential spectral absorption of the atmosphere, changing the spectral distribution of the downwelling shortwave flux. In this paper the term "surface albedo" refers to the apparent broadband albedo, and the albedo retrieval procedure presented here estimates the directional-hemispherical apparent broadband albedo.

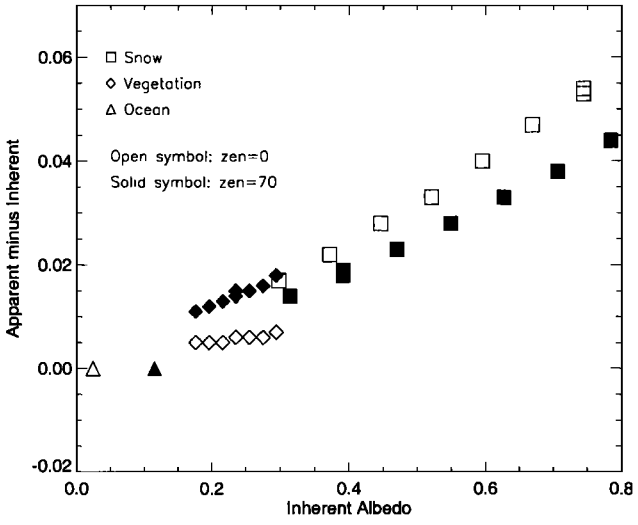

Figure 5. The difference between the apparent (atmosphere dependent) and inherent surface albedos of unfrozen ocean, snow-free land (vegetation), and snow. Data are from radiative transfer model calculations for a precipitable water amount of 0.5 cm, aerosol optical depth of 0.05, and solar zenith angles of 0^0 and 70^0.

The first step in the retrieval of clear-sky surface albedo is to convert the narrowband reflectances in AVHRR channels 1 and 2 to a TOA broadband (0.28 - 4.0 μm) reflectance. This is necessary because the anisotropic reflectance correction procedure (next step) requires a broadband reflectance. *Li and Leighton* [1992] (hereinafter LL92) developed a narrow to broadband conversion with coincident AVHRR and ERBE data for ocean, land, and ice/snow surfaces. *Csiszar and Gutman* [1999] use the method developed by *Hucek and Jacobowitz* [1995] for land surfaces, which is also based on AVHRR and ERBE measurements. Here the narrow-to-broadband conversion takes the same form as in those studies:

$$\rho_{toa} = a + b\rho_{1,toa} + c\rho_{2,toa}, \quad (1)$$

where $\rho_{1,toa}$ is the channel 1 reflectance, $\rho_{2,toa}$ is the channel 2 reflectance, ρ_{toa} is the broadband TOA reflectance, and *a*, *b*, and *c* are regression coefficients. To develop the regression relationship, Streamer was used to simulate the TOA reflectances over a broad range of viewing and illumination angles, atmospheric conditions (aerosol optical depth and water vapor amount), and surface types and albedos. In this step the model uses the discrete ordinate radiative transfer (DISORT) solver [*Stamnes et al.*, 1988] with eight streams. Streamer uses only directional-hemispherical spectral albedos for snow, so that variations in reflectance due to illumination geometry are captured, but variations due to viewing geometry are only a function of the atmospheric characteristics. However, because the coefficients in (1) are not a function of viewing or illumination conditions, the uncertainty resulting from this modeling limitation is expected to be small. For snow/ice surfaces, *a*, *b*, and *c* have values of 0.0215773, 0.277479, and 0.506755, respectively. For open ocean the broadband reflectance is set to the channel 1 reflectance.

The narrow to broadband conversion method presented in LL92 for snow/ice results in broadband values in the range of 4-8% higher than those computed here. The reason for this discrepancy is unclear. The approach used in LL92 avoids model biases that may exist here, but their limited temporal sample (4 days in July) may result in an observational bias for conditions outside of their sample. The time-dependent calibration of AVHRR channels 1 and 2, necessary to account for sensor drift, is an additional source of uncertainty. The LL92 coefficients are undoubtedly more accurate for their sample data set, but it is not clear how applicable they are to other NOAA satellites and to a broader range of conditions.

The next step is to correct for the dependence of the Sun-satellite-surface geometry on reflectance. This is done with data given by *Suttles et al.* [1988]. That study used ERBE and GOES data to determine TOA anisotropic reflectance factors (ARF) for the broad shortwave band over various surfaces. It updates the earlier work of *Taylor and Stowe* [1984]. Both the ERBE and GOES instruments measure radiances and are therefore a function of viewing and illumination geometry. To convert the directional reflectance to albedo, the ERBE/GOES ARFs are used:

$$\alpha_{toa} = \frac{\rho_{toa}}{f}, \tag{2}$$

where ρ_{toa} is the reflectance observed at the sensor (simulated in step 1), f is the anisotropic reflectance factor, and α_{toa} is the TOA albedo, which is only a function of solar zenith angle. A trilinear interpolation routine was used to obtain f as a function of satellite zenith angle, solar zenith angle, and the relative azimuth angle.

Next, the broadband, clear-sky, apparent surface albedo is estimated with a regression relationship of the form

$$\alpha_{toa} = a + b\alpha_s, \tag{3}$$

where α_s is the surface reflectance, and *a* and *b* are a function of water vapor, aerosol amount, and solar zenith angle. The coefficients were determined with the radiative transfer model for a variety of surface and atmospheric conditions and illumination angles. Viewing geometry was taken into account in the previous step and is therefore not relevant in this step. Snow/ice and vegetation surface types were used in the radiative transfer calcula-

Table 1. Atmospheric Correction Coefficients for Land and Snow/Ice (Equation 3)

Solar Zenith Cosine	*a, b:* PW=0.5 g cm^{-2} τ_{aer}=0.05	*a, b:* PW=0.5 g cm^{-2} τ_{aer}=0.5	*a, b:* PW=5.0 g cm^{-2} τ_{aer}=0.05	*a, b:* PW=5.0 g cm^{-2} τ_{aer}=0.5
1.00	0.03695, 0.77166	0.04406, 0.45630	0.03018, 0.74553	0.01463, 0.62228
0.95	0.03931, 0.76815	0.04915, 0.44979	0.03282, 0.74201	0.02173, 0.61429
0.90	0.04202, 0.76390	0.05450, 0.44280	0.03582, 0.73771	0.02963, 0.60501
0.85	0.04494, 0.75964	0.06070, 0.43445	0.03909, 0.73316	0.03798, 0.59530
0.80	0.04810, 0.75499	0.06716, 0.42603	0.04267, 0.72821	0.04719, 0.58482
0.75	0.05158, 0.74983	0.07414, 0.41706	0.04649, 0.72314	0.05691, 0.57361
0.70	0.05564, 0.74357	0.08197, 0.40686	0.05078, 0.71728	0.06782, 0.56104
0.65	0.05989, 0.73769	0.09030, 0.39632	0.05563, 0.71077	0.07953, 0.54765
0.60	0.06484, 0.73029	0.09958, 0.38445	0.06112, 0.70337	0.09242, 0.53278
0.55	0.07029, 0.72219	0.11005, 0.37048	0.06755, 0.69453	0.10665, 0.51609
0.50	0.07705, 0.71229	0.12161, 0.35574	0.07455, 0.68516	0.12220, 0.49827
0.45	0.08433, 0.70159	0.13448, 0.33943	0.08301, 0.67375	0.13953, 0.47827
0.40	0.09331, 0.68796	0.14911, 0.32035	0.09260, 0.66121	0.15892, 0.45536
0.35	0.10384, 0.67232	0.16544, 0.29988	0.10434, 0.64559	0.18016, 0.43075
0.30	0.11669, 0.65322	0.18419, 0.27680	0.11834, 0.62741	0.20387, 0.40307
0.25	0.13272, 0.62916	0.20543, 0.25065	0.13603, 0.60412	0.23016, 0.37195
0.20	0.15329, 0.59835	0.22964, 0.22240	0.15845, 0.57540	0.25882, 0.33787
0.15	0.18077, 0.55602	0.25720, 0.19178	0.18845, 0.53672	0.28921, 0.30073
0.10	0.21968, 0.49515	0.28783, 0.16234	0.23022, 0.48396	0.31943, 0.26212
0.05	0.27906, 0.39838	0.32097, 0.13823	0.29284, 0.40207	0.34524, 0.22090

tions, and the regression coefficients are based on the combined surface type data. There is a different set of coefficients for each solar zenith angle (cosines from 0.05 to 1.0 in increments of 0.05), aerosol visible optical depth (0.05 and 0.5), and precipitable water (0.5 and 5.0 cm) bin (Table 1). Ozone amount was prescribed at 325 Dobson units. Coefficients for conditions between the table values are linearly interpolated. This method was used by *Koepke* [1989] for AVHRR channels 1 and 2 separately. For the ocean surface albedo a simpler approach is used:

$$\alpha_s = a + b\alpha_{toa} + c\cos Z + dPW + e\tau_{aer}, \quad (4)$$

where PW is precipitable water (centimeters), τ_{aer} is aerosol visible optical depth (unitless), Z is the solar zenith angle, and a, b, c, d, and e are regression coefficients based on modeled albedos with values of -0.112236, 0.948389, 0.108496, 0.00242575, and -0.125026, respectively. The atmospheric correction method presented by *Li and Garand* [1994] was evaluated but was found to overestimate the atmospheric effect at large solar zenith angles.

The albedo of cloudy pixels is determined using the clear-sky albedo, interpolated to fill in the entire image, adjusted by the cloud optical depth and the solar zenith angle. This conversion is also based on model calculations, where the radiative transfer model was used to compute upwelling and downwelling fluxes for a snow/ice surface over a range of cloud and atmospheric conditions. A subset of those calculations was used to construct Figure 4. In the model calculations of steps 1, 3, and 4, the snow and vegetation visible albedos ranged from 0.5 to 0.99 and 0.07 to 0.15, respectively.

Based on the model results the derived relationship between the clear-sky broadband albedo, cloud optical depth, and the cloudy-sky broadband surface albedo of snow/ice is

$$\alpha_{s,\,cld} = a + b\alpha_{s,\,clr} + c\ln(\tau + 1) + d\cos Z, \quad (5)$$

where τ is the cloud visible optical depth (unitless), $\alpha_{s,clr}$ is the clear sky apparent surface albedo, Z is the solar zenith angle, and a, b, c, and d are regression coefficients with values -0.0491243, 1.06756, 0.0217075, and 0.0179505, respectively. Cloud optical depth retrievals are discussed in the next section. Aerosol and water vapor amounts are not explicit in this relationship because their effect on the surface albedo is small relative to that of clouds and because the adjustment is to the apparent albedo, which already includes their effects. No distinction is made between water and ice clouds, although both were included in the model data for the regression analysis.

The relationship works best when the snow surface is bright ($\alpha > 0.5$) and clouds have small to moderately large optical depths ($1 < \tau < 50$). The cloudy-sky albedo calculated with (5) will not be exactly the same as the clear albedo for a cloud optical depth of zero (clear sky). This is an artifact of the regression analysis and does not present a problem in the application of (5) because it should only be used when a scene is identified as cloudy. The sensitivity of (5) to cloud optical depth is such that a 50% error in optical depth results in a cloudy-sky surface albedo error of approximately 0.5% absolute at an optical depth of 1, and errors in the range of 1-2% for larger optical depths. The sensitivity to errors in the clear-sky albedo is higher, of the order of 4-9% absolute for a 10% error in the clear-sky albedo retrieval.

While much of the clear-sky albedo retrieval methodology is specific to the AVHRR (but could be adapted to other sensors), the cloudy-sky adjustment expressed in (5) is independent of the sensor type and characteristics. It could therefore be used with other satellite sensors or with nonsatellite data sets. Additionally, it was developed using a wide range of solar zenith angles (0° to 85°) and snow surface albedos, so it should be applicable to snow-covered areas outside of the polar regions.

4. Application

In this section we apply the clear-sky algorithm and the cloudy-sky adjustment to the full year of SHEBA data. The AVHRR data set is a product of the AVHRR Polar Pathfinder project [*Maslanik et al.*, 1997]. Global area coverage data acquired from overpasses nearest 1400 local solar time (2400 UTC) were regridded to a 5 km pixel size. Shortwave bands (channels 1 and 2), which are not calibrated on board, were calibrated to account for in-orbit degradation according to the method of *Rao* [1993] with updates available on the Web (http://psbsgi1.nesdis.noaa.gov:8080/EBB/ml/niccal2.html). For this study, data from NOAA 14 are used.

Before applying the surface albedo procedures we briefly describe the cloud retrievals. Cloud detection and optical depth retrievals with the AVHRR utilize reflectances at 0.9 and 3.7 μm as well as differences in brightness temperatures at 11 and 12 μm. Reflectance at 3.7 μm, which also contains an emitted thermal component, is approximated by removing from the total radiance an estimate of the emitted portion based on the temperature at 11 μm:

$$\rho_3 = \frac{L_3 - B_3(T_4)}{L_0\mu - B_3(T_4)}, \quad (6)$$

where ρ_3 is the channel 3 reflectance, L_3 is the channel 3 radiance, $B_3(T_4)$ is the Planck function for channel 3 based on the channel 4 temperature T_4, L_0 is the solar constant for the band adjusted for Earth-Sun distance, and μ is the cosine of the solar zenith angle. *Roger and Vermote* [1998] present an alternative method of estimating the 3.7 μm reflectance where the channel 3 thermal radiance is parameterized as a function of the channels 4 and 5 brightness temperature difference in nighttime imagery. While this may be a more realistic approach, *X. Xiong* (Evaluating the principles of cloud remote sensing with AVHRR and MAS imagery over SHEBA, submitted to *Journal of Geophysical Research*, 2000) found that the difference between the two methods in estimating the thermal radiance for an Arctic case study was less than 5%.

All clouds are considered to be either water or ice; no attempt is made to identify mixed phase or multilayer clouds. Cloud detection is accomplished with spectral threshold tests, as described by *Key* [2000]. The determination of cloud particle thermodynamic phase is based on both physical and spectral properties as described in *Key and Intrieri* [2000]. Cloud optical depth retrievals are done using a comprehensive database of modeled reflectances and brightness temperatures covering a wide range of surface and atmospheric conditions. The basic approach for daytime retrievals of water cloud follows that of *Nakajima and King* [1990], who showed that reflectances at absorbing wavelengths (e.g., 3.7 μm) are primarily dependent upon particle size while reflectances at nonabsorbing wavelengths (e.g., 0.6 or 0.9 μm) are more a function of optical depth. Reflectances at 0.9 and 3.7 μm were modeled with Streamer and DISORT, parameterized cloud and aerosol optical

properties, and gaseous absorption. Water cloud optical properties are based on Mie theory; ice cloud optical properties are based on ray-tracing results for hexagonal crystals [*Key and Schweiger*, 1998]. For ice clouds during the day the 3.7 μm reflectance is so small that it is unreliable. Therefore, 11 and 12 μm brightness temperatures are used to obtain a range of possible solutions, and the 0.9 μm reflectance is used to constrain the solution. Brightness temperature differences are also used to constrain the solution for thin water cloud over snow when the solution based on reflectances alone may not be unique. These procedures are detailed by *Key* [1995] and *Key* [2000]. A similar methodology has been used to retrieve water cloud optical depth in the Arctic by *Han et al.* [1999].

The AVHRR data are processed as follows. The cloud detection procedure is applied to identify clear and cloudy pixels. No subpixel cloud fraction is estimated. The surface albedo is then retrieved for clear areas using precipitable water amount from the SHEBA ship radiosonde profiles and climatological values for aerosol optical depth (0.06). Because the cloudy-sky albedo calculation is an adjustment to a clear-sky albedo value, cloudy pixels are filled with a weighted mean of nearby clear-sky albedos. The weighting is done with a kriging procedure that utilizes the spatial autocovariance of the field and thereby weights the data based on the degree and type of spatial variation with distance. The procedure will expand the search radius from the cloud pixel as far as necessary to find clear pixels, the only restriction being that the clear pixels must be of the same surface type. In practice, clear pixels are usually found within 100 km. Finally, the cloudy-sky adjustment to the clear-sky albedo is applied to cloudy pixels. All results shown below are averages of 5 x 5 pixel boxes (25 x 25 km) centered on the SHEBA ship location.

Due to uncertainties in plane parallel radiative transfer model results at large solar zenith angles, it is recommended that albedo retrievals be done only for solar zenith angles less than approximately 85°. In fact, a value of 75° may be more appropriate because of uncertainties in cloud optical depth retrieval for low Sun conditions. Figure 6 shows the latitudes and times of the year where solar zenith angles greater than 75° and 85° are experienced.

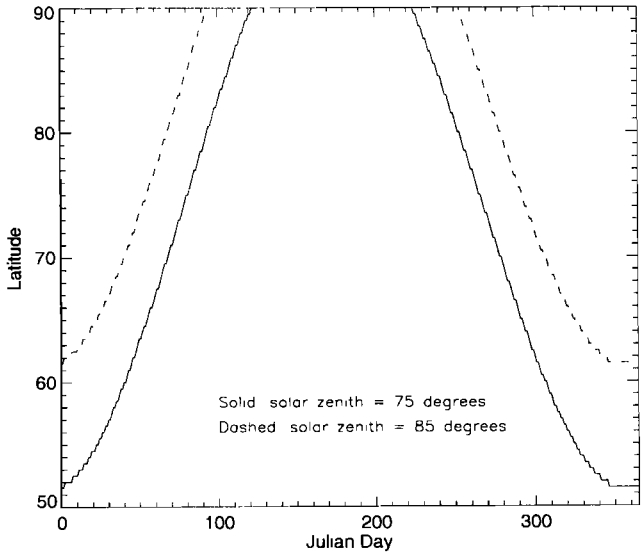

Figure 6. Latitudes and times of the year where zenith angles greater than 85° and greater than 75° are experienced at solar noon. All latitudes poleward of those shown will have solar zenith angles larger than 85° or 75°. The 85° line is relevant to albedo retrievals; the 75° line is relevant to cloud optical depth retrievals.

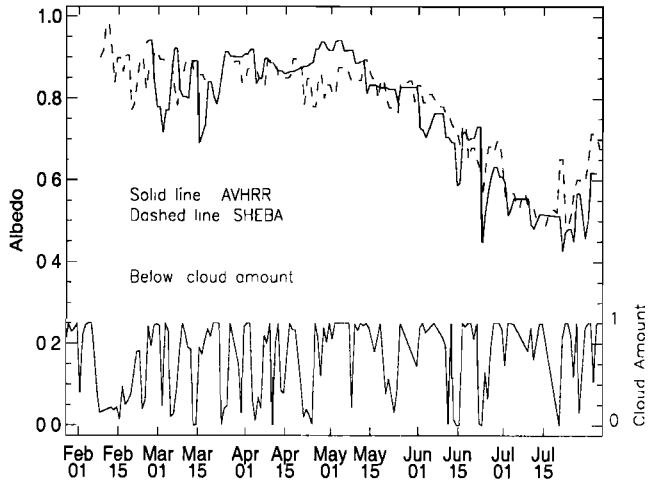

Figure 7. Time series of clear- and cloudy-sky surface albedo for the SHEBA ship location from surface shortwave flux measurements (dashed line) and from the AVHRR retrievals for the area around the ship (solid line). Also shown is the AVHRR-derived cloud amount (solid line at bottom; scale at right).

Figure 7 shows a time series of surface broadband albedo as measured at the surface with broadband shortwave downlooking and uplooking radiometers and as retrieved from the AVHRR. The SHEBA year started in the fall of 1997 and continued through the early fall of 1998. No surface measurements are available for the first part of the time series and November through early February was dark, so only the February through July period is shown. Overall the agreement between the surface and satellite measurements is good, though the satellite retrievals show a small negative bias (lower albedo) overall. The figure clearly shows the seasonal cycle of albedo, with the high albedo of fresh snow during the late winter and spring giving way to the lower albedo of old, melting snow and bare ice during the summer. The relationship between changes in cloud amount and changes in surface albedo is evident in the later part of the time series but is relatively weak in February and March when the shortwave flux is small and albedo estimates have a higher uncertainty.

There are a number of factors that cause differences between the surface and satellite-derived albedos. Spatial variability of the surface and cloud cover always introduces uncertainty in point versus area comparisons. For example, sea ice leads (linear fractures exposing open water) and summer melt ponds in the AVHRR field of view would cause a negative bias in the satellite-derived albedos, given that the surface radiometers are located on pack ice. Leads and melt ponds in the AVHRR field of view may explain some of the larger daily differences as well. However, *Stroeve et al.* [2001] found that clear-sky albedo retrievals over Greenland using the methodology presented here also exhibited a negative bias, so the bias may be at least in part inherent in the algorithm. Cloud cover variability

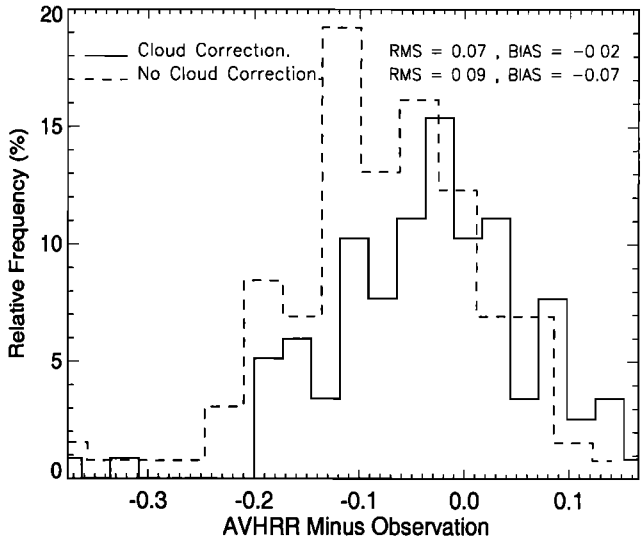

Figure 8. Relative frequency of differences between the AVHRR retrievals of surface albedo and the SHEBA ship measurements with (solid) and without (dashed) the cloudy-sky adjustment. The bias and root-mean-square errors are also given.

can cause either negative or positive biases; e.g., if the satellite-derived cloud cover is greater than that observed at the surface, the estimated albedo for the area will be higher than the observed albedo by virtue of the cloudy-sky adjustment.

A potentially more significant source of error results from inaccuracies in the top-of-atmosphere angular models of *Suttles et al.* [1988]. *Li* [1996] evaluated the performance of the ERBE angular models over the Arctic and found that those for snow and ice scenes have the largest uncertainty. *Stroeve et al.* [2001] also found that the angular models are a significant source of error in snow albedo retrievals. The difference in spectral ranges of the measured (0.285 - 2.8 μm) and computed (0.28 - 4.0 μm) shortwave fluxes results in an underestimate of less than 1% (absolute). Finally, the procedure that interpolates clear-sky albedos to cloudy areas will introduce large errors for pixels whose surface characteristics differ significantly from the nearby clear areas.

Figure 8 shows the frequency of differences between the AVHRR retrievals and the SHEBA ship measurements with and without the cloudy-sky adjustment for the entire time series. The bias (AVHRR minus surface observation) and root-mean-square errors (RMS) are also given. The bias without the adjustment for cloud cover is 0.065; with the adjustment it is 0.022. The difference between them (0.043) agrees well with the theoretical and observed effects of cloud cover noted previously: 0.04 to 0.06 for the SHEBA data shown in Figure 4 and 0.03 to 0.05 for cloud optical depths less than 50 with the theoretical snow albedo data in Figure 3.

The mean difference between cloudy- and clear-sky albedos of approximately 0.05 could be used as an overall adjustment to clear albedos in the absence of cloud optical depth information. For example, the surface albedo for cloudy areas in a data set of monthly mean clear-sky snow surface albedo could be estimated by simply adding 0.05 to a distance weighted mean of surrounding clear values. If the cloud cover within a cloudy grid cell is less than 100%, then the surface albedo would have to be further weighted by the cloud amount. The magnitude of the albedo correction (0.05) could, of course, be adjusted higher or lower to account for cloud type. However, given the effect of cloud optical thickness on snow albedo shown in Figure 3, if optical thickness is available then it should be used, especially in instantaneous retrievals.

5. Conclusions

The effect of clouds on the albedo of snow-covered surfaces is significant and should be considered in satellite retrievals. On the average the snow/ice albedo will be approximately 0.04 to 0.06 (or 4-6%, absolute) higher under cloud cover than for clear skies, with a range of slightly less than 0 to approximately 0.15. A method was presented for the retrieval of the cloudy-sky surface albedo of snow and ice using the AVHRR. The cloudy-sky albedo is estimated from the clear-sky albedo, cloud optical depth and the solar zenith angle, so that its application requires that cloud properties be estimated from the satellite data as well as the clear-sky albedo. The parameterization of the cloudy-sky albedo is not specific to the AVHRR and could therefore be used with other existing and future sensors and nonsatellite data sets.

An application of the algorithm to once-daily data from the SHEBA experiment for February through July 1998 demonstrated that the surface albedo of snow/ice can be obtained from space with an uncertainty of approximately 7% absolute. It was shown that the magnitude of the average cloudy-sky adjustment agrees well with the average effect of clouds observed in two surface data sets and calculated with a radiative transfer model. For surface albedo climatologies based on monthly average clear-sky values, it may be sufficient to make an adjustment for clouds by incorporating the mean cloud effect of 0.05, more or less depending on the frequency of thin and thick clouds. For studies that are done with instantaneous retrievals, we recommend that the procedures described in this paper be incorporated. The data and coded procedures presented here are part of the Cloud and Surface Parameter Retrieval system for polar AVHRR [*Key*, 2000], which can be obtained via the Web at http://stratus.ssec.wisc.edu.

Acknowledgments. This research was supported by NASA grants NAG5-8625, NAG5-4375, and NAG5-6666, and NSF grants OPP-9701757 and OPP-0096085. We thank J. Maslanik, T. Scambos, and T. Haran for all their work on the AVHRR Polar Pathfinder (APP) data set. The APP data set is available from the National Snow and Ice Data Center, Boulder, Colorado (http://www.nsidc.colorado.edu). We also thank O. Persson, R. Lindsay, and the other SHEBA scientists for their measurements of shortwave radiation during the field experiment.

References

Blanchet, J.-P., and R. List, Estimation of optical properties of Arctic haze using a numerical model, *Atmos. Ocean*, *21*(4), 444-465, 1983.

Csiszar, I., and G. Gutman, Mapping global land surface albedo from NOAA AVHRR, *J. Geophys. Res.*, *104*, 6215-6228, 1999.

DeAbreu, R.A., J. Key, J.A. Maslanik, M.C. Serreze, and E.F. LeDrew, Comparison of in situ and AVHRR-derived surface broadband albedo over Arctic sea ice, *Arctic*, *47*(3), 288-297, 1994.

Grenfell, T.C., and D.K. Perovich, Spectral albedos of sea ice and incident solar irradiance in the southern Beaufort Sea, *J. Geophys. Res.*, *89*, 3573-3580, 1984.

Hall, D.K., W.M. Kovalick, and A.T.C. Chang, Satellite-derived reflectance of snow-covered surfaces in northern Minnesota, *Remote Sens. Environ.*, *33*, 87-96, 1990.

Han, W., K. Stamnes, and D. Lubin, Remote sensing of surface and cloud properties in the Arctic from AVHRR measurements, *J. Appl. Meteorol., 39*, 989-1012, 1999.

Hucek, R., and H. Jacobowitz, Impact of scene dependence on AVHRR albedo models, *J. Atmos. Oceanic Technol., 12*, 697-711, 1995.

Key, J., Retrieval of cloud optical depth and particle effective radius at high latitudes using visible and thermal satellite data, in *Proceedings of the European Symposium on Satellite Remote Sensing II,SPIE J., 2578*, 318-325, 1995.

Key, J., The cloud and surface parameter retrieval (CASPR) system for polar AVHRR, 59 pp., Coop. Inst. for Meteorol. Satell. Stud., Univ. of Wisc., Madison, 2000.

Key, J., and J. Intrieri, Cloud particle phase determination with the AVHRR, *J. Appl. Meteorol., 36*(10), 1797-1805, 2000.

Key, J., and A.J. Schweiger, Tools for atmospheric radiative transfer: Streamer and FluxNet, *Comp. Geosci., 24*(5), 443-451, 1998.

Koepke, P., Removal of atmospheric effects from AVHRR albedos, *J. Appl. Meteorol., 28*, 1341-1348, 1989.

Li, Z., On the angular correction of satellite radiation measurements: The performance of ERBE angular dependence model in the Arctic, *J. Theor. Appl. Climatol., 54*, 235-248, 1996.

Li, Z., and L. Garand, Estimation of surface albedo from space: A parameterization for global application, *J. Geophys. Res., 99*, 8335-8350, 1994.

Li, Z., and H.G. Leighton, Narrowband to broadband conversion with spatially autocorrelated reflectance measurements, *J. Appl. Meteorol., 31*, 421-432, 1992.

Lindsay, R.W., and D.A. Rothrock, Arctic sea ice albedo from AVHRR, *J. Clim., 7*(11), 1737-1749, 1994.

Maslanik, J., C. Fowler, J. Key, T. Scambos, T. Hutchinson, and W. Emery, AVHRR-based polar pathfinder products for modeling applications, *Ann. Glaciol., 35*, 171-182, 1997.

Moritz, R.E., J.A. Curry, N. Untersteiner, and A.S. Thorndike, Prospectus: Surface heat budget of the Arctic Ocean, *NFSF-ARCSS OAII Tech. Rep. 3*, 33 pp., SHEBA Proj. Off., Polar Sci. Cent., Appl. Phys. Lab., Univ. of Wash., Seattle, 1993.

Nakajima, T., and M.S. King, Determination of the optical thickness and effective particle radius of clouds from reflected solar radiation measurements, I: Theory, *J. Atmos. Sci., 47*(15), 1878-1893, 1990.

Rao, C.R.N., Degradation of the visible and near-infrared channels of the advanced very high resolution radiometer on the NOAA-9 spacecraft: Assessment and recommendations for corrections, *NOAA Tech. Rep. NESDIS 70*, 25 pp., U.S. Dep. of Comm., Washington, D.C., 1993.

Roger, J.C., and E.F. Vermote, A method to retrieve the reflectivity signature at 3.75 microns from AVHRR, *Remote Sens. Environ., 64*, 103-114, 1998.

Stamnes, K., S.-C. Tsay, W. Wiscombe, and K. Jayaweera, Numerically stable algorithm for discrete-ordinate-method radiative transfer in multiple scattering and emitting layered media, *Appl. Opt., 27*, 2502-2509, 1988.

Stroeve, J., A. Nolin, and K. Steffen, Comparison of AVHRR-derived and in situ surface albedo over the Greenland ice sheet, *Remote Sens. Environ., 62*, 262-276, 1997.

Stroeve, J., J. Box, C. Fowler, T. Haran, J. Key, and J. Maslanik, Intercomparison between in situ and AVHRR Polar Pathfinder-derived surface albedo over Greenland, *Remote Sens. Environ.*, in press, 2001.

Suttles, J.T., R.N. Green, P. Minnis, G.L. Smith, W.F. Staylor, B.A. Wielicki, I.J. Walker, D.F. Young, V.R. Taylor, and L.L. Stowe, Angular radiation models for Earth-atmosphere system: volume I, Shortwave radiation, *NASA Ref. Pub. 1184*, 144 pp., 1988.

Taylor, V.R., and L.L. Stowe, Atlas of reflectance patterns for uniform Earth and cloud surfaces (NIMBUS-7 ERB-61 days), *NOAA Tech. Rep. NESDIS 10*, 66 pp., U.S. Dep. of Comm., Washington, D.C., 1984.

Wanner, W., A.H. Strahler, B. Hu, P. Lewis, J.-P. Muller, X. Li, C.L. Barker Schaaf, and M.J. Barnsley, Global retrieval of bidirectional reflectance and albedo over land from EOS MODIS and MISR data: Theory and algorithm, *J. Geophys. Res., 102*, 17,143-17,161, 1997.

C. Fowler, Colorado Center for Astrodynamics Research, University of Colorado, Boulder, CO 80309.

J.R. Key, Office of Research and Applications, National Environmental Satellite, Data, and Information Service, NOAA, Madison, WI 53706. (jkey@ssec.wisc.edu)

J.C. Stroeve, Cooperative Institute for Research in Environmental Sciences, University of Colorado, Boulder, CO 80309.

X. Wang, Cooperative Institute for Meteorological Satellite Studies, University of Wisconsin, Madison, WI 53706.

(Received September 18, 2000; revised January 9, 2001;
accepted January 26, 2001.)